to evaluate energy flux at the control-volume surface, are in very good agreement with the exact solution in Figs. 2a–2d. The moving shock wave is captured very sharply within a few nodes. The pressure and velocity solutions are almost exact, however, there is a minor undershoot before the contact discontinuity in the temperature distribution. Since the density is calculated from the equation of state, its value is completely dependent on the pressure and temperature fields. The effect of using Eqs. (7) and (11) to evaluate the energy flux at the control-volume surface is shown in Figs. 2e and 2f, respectively. The pressure and velocity distributions are not shown here; they are similar to the results in Figs. 2b and 2d, except that for the velocity distributions there exists a small overshoot at $x = 0.0$. A temperature undershoot higher than that in Figs. 2c and 2e is seen in Fig. 2f. However, there is not much difference in the rest of the temperature distributions; see Ref. 11 for complete results.

In conclusion, for the numerical results, the overall accuracy of the method is found to be quite satisfactory, and no particular problem has been detected. All three forms of the energy flux evaluation can be used in this method, however, smoother results are obtained when Eq. (9) is used.

Acknowledgments

The financial support of the Natural Sciences and Engineering Research Council of Canada is gratefully acknowledged. The first author would like to thank the Ministry of Culture and Higher Education of Iran for the scholarship he received.

References

[1]Montagne, J. L., Yee, C., and Vinokur, M., "Comparative Study of High Resolution Shock Capturing Schemes for Real Gas," *AIAA Journal*, Vol. 27, No. 10, 1989, pp. 1332–1346.

[2]Lin, H., and Chieng, C. C., "Characteristic-Based Flux Limiters of an Essentially Third-Order Flux Splitting Method for Hyperbolic Conservation Laws," *International Journal for Numerical Methods in Fluids*, Vol. 13, No. 3, 1991, pp. 287–307.

[3]Karki, K. C., and Patankar, S. V., "Pressure-Based Calculation Procedure for Viscous Flows at All Speeds in Arbitrary Configurations," *AIAA Journal*, Vol. 27, No. 9, 1989, pp. 1167–1174.

[4]Shyy, W., Chen, M. H., and Sun, C. S., "Pressure-Based Multigrid Algorithm for Flow at All Speeds," *AIAA Journal*, Vol. 30, No. 11, 1992, pp. 2660–2669.

[5]Schneider, G. E., and Karimian, S. M. H., "Advances in Control-Volume Based Finite-Element Methods for Compressible Flows," *Computational Mechanics*, Vol. 14, No. 5, 1994, pp. 431–446.

[6]Baliga, B. R., and Patankar, S. V., "A Control Volume Finite-Element Method for Two-Dimensional Fluid Flow and Heat Transfer," *Numerical Heat Transfer*, Vol. 6, No. 3, 1983, pp. 245–261.

[7]Schneider, G. E., and Raw, M. J., "Control-Volume Finite-Element Method for Heat Transfer and Fluid Flow Using Co-located Variables —1. Computational Procedure," *Numerical Heat Transfer*, Vol. 11, No. 4, 1987, pp. 363–390.

[8]Raw, M. J., Galpin, P. F., and Raithby, G. D., "The Development of an Efficient Turbomachinery CFD Analysis Procedure," AIAA Paper 89-2394, 1989.

[9]Naterer, G. F., and Schneider, G. E., "Use of the Second Law in a Predictive Capacity for Compressible Fluid Flow Discrete Analysis," AIAA, Washington, DC, 1992 (AIAA Paper 92-2942).

[10]Karimian, S. M. H., and Schneider, G. E., "Pressure-Based Computational Method for Compressible and Incompressible Flows," *Journal of Thermophysics and Heat Transfer*, Vol. 8, No. 2, 1994, pp. 267–274.

[11]Karimian, S. M. H., and Schneider, G. E., "Application of a New Control-Volume-Based Finite-Element Formulation to the Shock Tube Problem," AIAA Paper 94-0131, 1994.

[12]Van Doormaal, J. P., Turan, A., and Raithby, G. D., "Evaluation of New Techniques for the Calculation of Internal Recirculating Flows," AIAA Paper 87-0059, 1987.

[13]Rhie, C. M., and Chow, W. L., "Numerical Study of the Turbulent Flow Past an Airfoil with Trailing Edge Separation," *AIAA Journal*, Vol. 21, No. 11, 1983, pp. 1525–1532.

Simulating Heat Addition via Mass Addition in Constant Area Compressible Flows

W. H. Heiser,* W. B. McClure,† and C. W. Wood†
U.S. Air Force Academy, Colorado 80840

Introduction

THE one-dimensional flow analyses of this study demonstrate the interesting and potentially useful similarities between the influence of heat addition and of mass addition (injected normal to the flow at the same total temperature) on compressible duct flows.

For the most part, the effect of a given fractional mass flow addition on flow properties is equivalent to twice that amount of fractional total temperature increase. This conclusion applies in particular to the important phenomena of choking and wall boundary-layer separation, the latter resulting from the adverse pressure gradients created by heat or mass addition in supersonic flows. Wall boundary-layer separation is, in fact, so natural to such flows that it appears to often precede any choking that would otherwise occur.

The results of this study suggest that some aspects of the complex behavior of dual-mode ramjet/scramjet combustors[1] could be experimentally evaluated or demonstrated by replacing combustion with less expensive, more easily controlled, safer mass addition.

The first clue to the strength of the analogy is revealed by the well-known influence coefficients of one-dimensional compressible flows (e.g., Table 8.2 of Ref. 2), several of the most important of which are found in Table 1. The clear message of this tabulation is that the incremental influence of a given fractional change of mass flow rate $\delta\dot{m}/\dot{m}$ on Mach number M, static pressure p, and total pressure p_t is exactly double that of an equal fractional change of total temperature $\delta T_t/T_t$ for the same ratio of specific heats γ.

Simple Mass or Heat Addition Flows

The analyses that follow next are based on the classical one-dimensional model of the steady, constant throughflow area flow of a calorically perfect gas.[2] In addition to the traditional model, it will be assumed that any mass addition has the same total temperature and imposition as the inlet flow and is injected normal to the duct axis (i.e., without contributing to the axial momentum) and, unless otherwise noted, the flow is frictionless.

The reader will recognize that many of these assumptions are made for convenience, rather than out of necessity. Solutions to the governing equations could be obtained with less restrictive assumptions (e.g., the case of combined mass addition and wall friction that appears later) but at a price we believe to be disproportionate to the benefit, including the loss of simplicity and transparency. These assumptions have led to fruitful results throughout the history of compressible fluid mechanics, as they will for the situation at hand.

When the throughflow area is constant and only one forcing function (e.g., heat or mass addition) is present, these flows are commonly known as simple flows. They have many appealing and useful characteristics, the best known being that they yield closed-form algebraic solutions that depend on the single forcing function (e.g., Table 8.3 of Ref. 2). Simple flows have contributed generously to organizing our thinking, intuition, and experiences about compressible flows, and the present case will prove to be no exception. The simple flow involving heat addition is usually referred to as Rayleigh flow. The simple flow involving mass addition has no established designation, and will be referred to here as SMA flow.

The solution procedures for Rayleigh flow and SMA flow will not be reproduced in any detail here, but the same solutions can be

Received Oct. 18, 1993; revision received June 15, 1994; accepted for publication June 15, 1994.

*Professor, Department of Aeronautics. Fellow AIAA.
†Associate Professor, Department of Aeronautics. Senior Member AIAA.

Table 1 Influence coefficients for heat and mass addition in one-dimensional compressible flows.

	$\frac{dT_t}{T_t}$	$\frac{d\dot{m}}{\dot{m}}$
$\frac{dM}{M}$	$\frac{(1+\gamma M^2)\{1+[(\gamma-1)/2]M^2\}}{2(1-M^2)}$	$\frac{(1+\gamma M^2)\{1+[(\gamma-1)/2]M^2\}}{1-M^2}$
$\frac{dp}{p}$	$-\frac{\gamma M^2\{1+[(\gamma-1)/2]M^2\}}{1-M^2}$	$-\frac{2\gamma M^2\{1+[(\gamma-1)/2]M^2\}}{1-M^2}$
$\frac{dp_t}{p_t}$	$-\frac{\gamma M^2}{2}$	$-\gamma M^2$

obtained in a number of ways, the most convenient being the manipulation of established formulas for simple flows (e.g., columns 2 and 4 of Table 8.3 of Ref. 2) and subsequent application of the useful integral relations.[2] [A perceptive reviewer familiar with Ref. 2 suggested that SMA flows be referred to as SMA-0 flows (corresponding to $y = 0$), because SMA-1 flows (corresponding to $y = 1$) display a similar analogy between area variation and mass addition.]

It is important to emphasize that the simple flow solutions for the exit conditions (subscript e) depend solely upon the inlet conditions (subscript i) and the cumulative fractional change of either total temperature $\delta T_t/T_{ti}$ or mass flow $\delta\dot{m}/\dot{m}_i$. They do not require integration and do not depend on the axial distribution of the addition of either heat or mass.

Simple Mass Addition (SMA) Flow

When only mass addition is present (and $\delta T_t = 0$), then

$$M_e^2 = \frac{1 - 2\gamma\Gamma^2 \pm \sqrt{1 - 2(\gamma+1)\Gamma^2}}{2\gamma^2\Gamma^2 - (\gamma - 1)} \tag{1}$$

where + and − correspond to $M_e > 1$ and $M_e < 1$, respectively, and

$$\Gamma = \frac{[1 + (\delta\dot{m}/\dot{m}_i)]M_i\sqrt{1 + [(\gamma-1)/2]M_i^2}}{1 + \gamma M_i^2}$$

and the other leading properties are found from

$$\frac{p_e}{p_i} = \frac{1 + \gamma M_i^2}{1 + \gamma M_e^2} \tag{2}$$

$$\frac{p_{te}}{p_{ti}} = \frac{p_e}{p_i} \cdot \left\{\frac{1 + [(\gamma-1)/2]M_e^2}{1 + [(\gamma-1)/2]M_i^2}\right\}^{\gamma/(\gamma-1)} \tag{3}$$

$$\frac{T_e}{T_i} = \frac{1 + [(\gamma-1)/2]M_i^2}{1 + [(\gamma-1)/2]M_e^2} \tag{4}$$

Choking

The influence coefficient in Table 1 indicates that adding mass always drives the Mach number toward 1 or choking. This outcome is intuitively appealing because it resembles the familiar simple flow cases of heat addition or skin friction. There is an upper limit to the fractional amount of mass that can be added before choking at the exit is encountered and the inlet conditions can no longer be sustained. The expression for that limit, obtained by setting $M_e = 1$ (or the discriminant = 0) in Eq. (1), is

$$\left(\frac{\delta\dot{m}}{\dot{m}_i}\right)_c = \frac{1 + \gamma M_i^2}{M_i\sqrt{2(\gamma+1)\left\{1 + [(\gamma-1)/2]M_i^2\right\}}} - 1 \tag{5}$$

where the subscript c refers to choking.

The results of calculations based on these solutions are presented as continuous lines in Fig. 1. They are shown for two typical dual-mode combustor inlet Mach numbers and for their entire respective allowable ranges of fractional mass addition. This information, at the very least, reveals that large variations in important and easily measured flow properties can be caused by relatively small fractional mass flow additions. It also confirms the Table 1 influence coefficient conclusion that a major difference between supersonic and subsonic SMA flow is the sign of the static pressure change.

Wall Boundary-Layer Separation

The static pressure increase resulting from mass addition for supersonic inlet flows could cause the wall boundary layer to separate, and the assumptions and model of this analysis to break down. An indication of the minimum amount of fractional mass flow addition required to make this happen can be obtained by applying the most elementary version of the Stratford turbulent boundary-layer separation criterion, namely, that separation will occur when the pressure coefficient (i.e., the overall static pressure rise divided by the inlet dynamic pressure q_i)

$$C_p = \frac{p_e - p_i}{q_i} = \frac{2[(p_e/p_i) - 1]}{\gamma M_i^2} \tag{6}$$

exceeds a set value.[3] Experimental evidence suggests that C_p will be in the vicinity of 0.40 for this type of flow. Although this approach is unlikely to yield precise predictions, it is employed here in the spirit that it can be expected to lead to reasonable figures and realistic trends.

Combining only Eqs. (2) and (6) leads to the result that

$$\left(\frac{M_e}{M_i}\right)_s = \sqrt{\frac{2 - C_p}{2 + \gamma C_p M_i^2}} \tag{7}$$

where the subscript s refers to separation, so that, using Eq. (1)

$$\left(\frac{\delta\dot{m}}{\dot{m}_i}\right)_s = \sqrt{\frac{1 - (C_p/2)}{1 + [(\gamma-1)/2]M_i^2}\left\{1 + \left[(\gamma-1) + \frac{\gamma+1}{2}C_p\right]\frac{M_i^2}{2}\right\}} - 1 \tag{8}$$

Interestingly, these expressions also lead to the conclusion that the axial velocity ratio

$$\left(\frac{V_e}{V_i}\right)_s = \frac{1 - (C_p/2)}{1 + (\delta\dot{m}/\dot{m}_i)_s} \tag{9}$$

is very close in appearance to the diffusion factor separation criterion often applied by engineers to similar flow situations, all the more so because the maximum value of $\delta\dot{m}/\dot{m}_i$ is much less than 1 (see Fig. 1).

A comparison of the fractional mass additions expected to cause choking and separation for given inlet Mach numbers is found as the continuous lines in Fig. 2. This information suggests that separation is likely to precede choking for most supersonic turbulent SMA flows, and, in turn, implies that it is very likely to happen if the flow

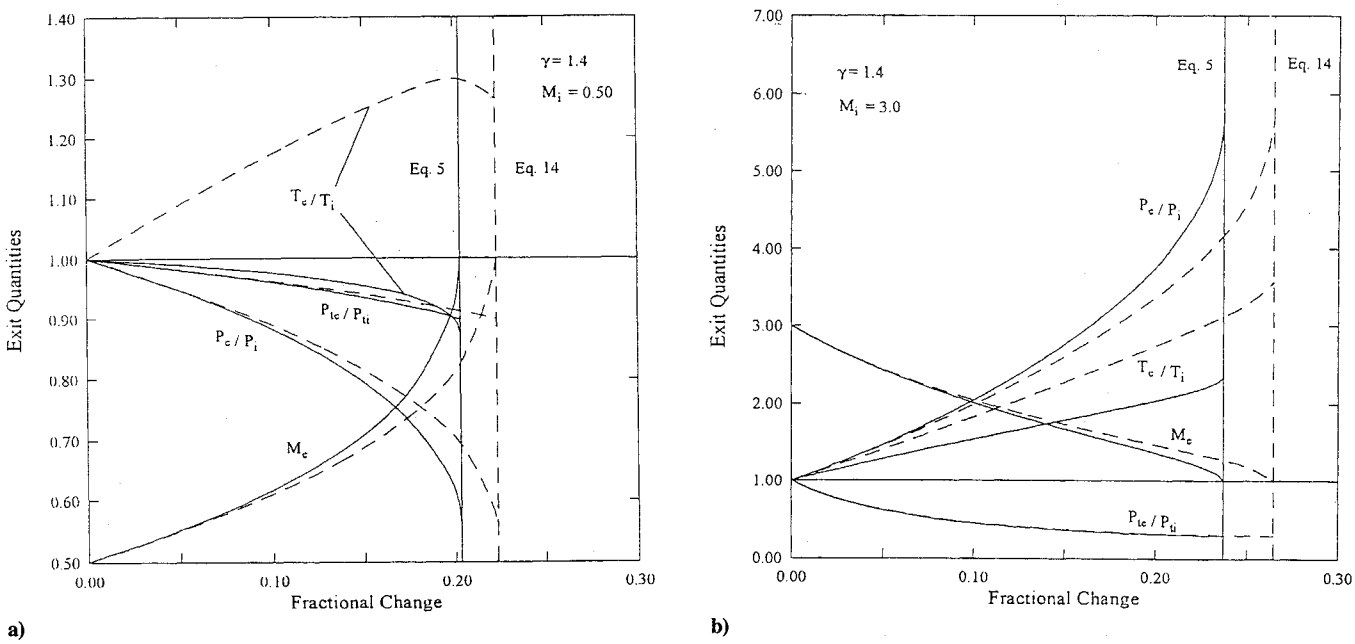

Fig. 1 Comparison of flow property behavior for SMA and Rayleigh flows, horizontal axis fractional change refers either to $\delta\dot{m}/\dot{m}_i$ or $\frac{1}{2}(\delta T_t/T_{ti})$; a) subsonic flow and b) supersonic flow. Mass addition: continuous lines, heat addition: broken lines.

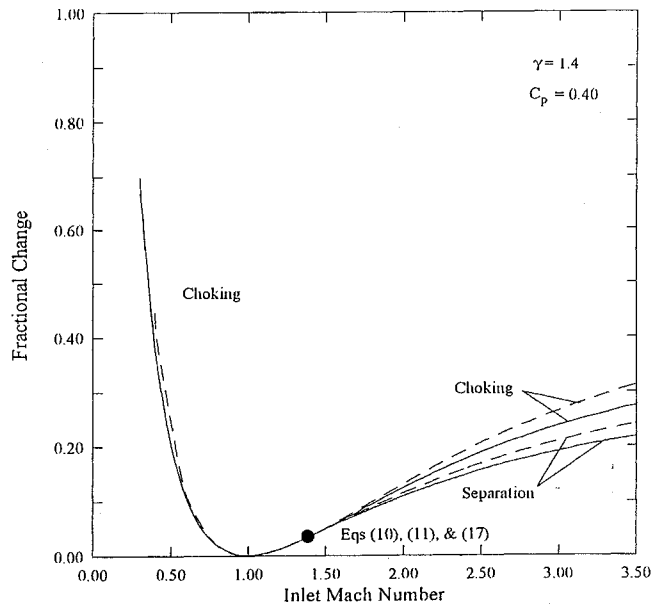

Fig. 2 Comparison of choking and separation limits for SMA and Rayleigh flows, vertical axis fractional change refers either to $\delta\dot{m}/\dot{m}_i$ or $\frac{1}{2}(\delta T_t/T_{ti})$.

remains laminar and the allowable C_p is even smaller. Note that the curves intersect where $M_{e,s} = 1$, or, using Eq. (7)

$$(M_i)_{c,s} = \sqrt{\frac{2}{2-(\gamma+1)C_p}} \tag{10}$$

$$\left(\frac{\delta\dot{m}}{\dot{m}_i}\right)_{c,s} = \frac{1-(C_p/2)}{\sqrt{1-C_p}} - 1 \tag{11}$$

to the left of which either point so little mass flow addition is needed to cause choking that turbulent separation cannot occur or the static pressure decreases due to mass addition in subsonic flow.

Rayleigh Flow

When only heat addition or total temperature increase is present (and $\delta\dot{m} = 0$), then

$$M_e^2 = \frac{1-2\gamma\Omega \pm \sqrt{1-2(\gamma+1)\Omega}}{2\gamma^2\Omega-(\gamma-1)} \tag{12}$$

where + and − correspond to $M_e > 1$ and $M_e < 1$, respectively, and

$$\Omega = \left(1+\frac{\delta T_t}{T_{ti}}\right)\left\{\frac{M_i^2\left\{1+[(\gamma-1)/2]M_i^2\right\}}{\left(1+\gamma M_i^2\right)^2}\right\}$$

and the other leading properties are found from Eqs. (2) and (3) and

$$\frac{T_e}{T_i} = \left(1+\frac{\delta T_t}{T_{ti}}\right)\left\{\frac{1+[(\gamma-1)/2]M_i^2}{(1+[(\gamma-1)/2]M_e^2}\right\} \tag{13}$$

Choking

The influence coefficient in Table 1 indicates that adding heat always drives the Mach number toward 1 or choking. This is the origin of the thermal choking phenomenon. There is an upper limit to the fractional amount of total temperature increase that can occur before choking at the exit is encountered and the inlet conditions can no longer be sustained. The expression for that limit, obtained by setting $M_e = 1$ (or the discriminant = 0) in Eq. (12), is

$$\left(\frac{\delta T_t}{T_{ti}}\right)_c = \frac{\left(1+\gamma M_i^2\right)^2}{2(\gamma+1)M_i^2\left\{1+[(\gamma-1)/2]M_i^2\right\}} - 1 \tag{14}$$

The results of calculations based on these solutions are presented as the broken lines in Fig. 1. They are shown for two typical dual-mode combustor inlet Mach numbers and for their entire respective allowable ranges of fractional total temperature increase. Their most striking feature is their close resemblance to those of SMA flow, except, for obvious reasons, the static temperature ratio T_e/T_i [see Eqs. (4) and (13)]. One can hardly escape the conclusion that SMA flow can provide a close analogy to Rayleigh flow.

Wall Boundary-Layer Separation

The static pressure increase resulting from heat addition for supersonic inlet flows could cause the wall boundary layer to separate, and the assumptions and model of this analysis to break down. This effect is, in fact, usually found in dual-mode combustor experimental data during high heat release supersonic combustion operation.[1] Fortuitously, the available data also seem to support the use of the elementary Stratford turbulent boundary-layer separation criterion

with a $C_p \sim 0.40$ despite the unusual circumstances of this application. We will, therefore, use it again as a general indicator of the behavior of Rayleigh flow.

Application of this criterion leads to the same result as Eq. (7), so that, using Eq.(12)

$$\left(\frac{\delta T_t}{T_{ti}}\right)_s = \frac{1-(C_p/2)}{1+[(\gamma-1)/2]M_i^2} \times \left\{1+\left[(\gamma-1)+\frac{\gamma+1}{2}C_p\right]\frac{M_i^2}{2}\right\}-1 \tag{15}$$

Interestingly, the governing equations also lead to the conclusion that

$$\left(\frac{V_e}{V_i}\right)_s = 1-\frac{C_p}{2} \tag{16}$$

which is identical in appearance to the diffusion factor separation criterion often applied by engineers to diffusers and turbomachinery blading.

A comparison of the fractional total temperature increases expected to cause choking and separation for given inlet Mach numbers is found as the broken lines in Fig. 2. This information suggests that separation is likely to precede choking for supersonic turbulent Rayleigh flows and, in turn, implies that it is very likely to happen if the flow remains laminar and the allowable C_p is even smaller. Note that the curves intersect at the point where $M_{e,s} = 1$, as given by Eq. (10) and

$$\left(\frac{\delta T_t}{T_{ti}}\right)_{c,s} = \frac{[1-(C_p/2)]^2}{1-C_p} - 1 \tag{17}$$

to the left of which point so little heat addition is needed to cause choking that turbulent separation cannot occur.

Again, the close likenesses in Fig. 2 show that there is a strong analogy between SMA flow and Rayleigh flow.

Combined Mass Addition and Wall Friction

Having established the close correspondence between SMA flow and Rayleigh flow, the next step is to consider the realities of designing experiments. We will, therefore, now estimate the influence of wall friction on what would otherwise be an SMA flow. This case is not found in the classical literature but can be easily done by including a wall friction resistance force in the control volume analysis.

To simplify the analysis, nevertheless maintaining adequate accuracy, the wall friction force is based entirely upon the inlet conditions, rather than on a local skin friction integral from inlet to exit. Thus, the total duct wall friction force is given by the expression

$$F_f = 4f\frac{L}{D}\cdot q_i \cdot A = 2f\frac{L}{D}\cdot \gamma M_i^2 \cdot p_i \cdot A \tag{18}$$

where f is a friction coefficient based primarily on the Reynolds number of the flow, and the duct aspect ratio L/D is the ratio of the length to the hydraulic diameter (i.e., four times the throughflow area A divided by its circumference which, for a circular duct, is equal to the geometric diameter and, for a planar duct, is equal to twice the passage height). The selection of this model is warranted for two reasons. First, as will be shown later, the local dynamic pressure does not ordinarily vary much from inlet to exit and the average dynamic pressure varies even less. Second, f can only be estimated in advance within fairly wide limits, thus frustrating any efforts to obtain very precise estimates.

When the wall friction force is included, the constant area control volume analysis yields

$$M_e^2 = \frac{1-2\gamma\Lambda^2 \pm \sqrt{1-2(\gamma+1)\Lambda^2}}{2\gamma^2\Lambda^2-(\gamma-1)} \tag{19}$$

where + and − correspond to $M_e > 1$ and $M_e < 1$, respectively, and

$$\Lambda = \frac{[1+(\delta\dot{m}/\dot{m}_i)]M_i\sqrt{1+[(\gamma-1)/2]M_i^2}}{1+\gamma M_i^2[1-2f(L/D)]}$$

and the static pressure ratio is given by

$$\frac{p_e}{p_i} = \frac{1+\gamma M_i^2[1-2f(L/D)]}{1+\gamma M_e^2} \tag{20}$$

while the total pressure ratio and static temperature ratio are given by Eqs. (3) and (4), respectively. Note that the prior SMA flow results are obviously recovered when f is zero.

Choking

Since friction also drives M_e toward 1, the maximum possible fractional mass addition allowed before choking occurs at the exit will be less than for SMA flow. The expression for that limit at a given value of $f(L/D)$, obtained by setting $M_e = 1$ (or the discriminant = 0) in Eq. (19), is

$$\left(\frac{\delta\dot{m}}{\dot{m}_i}\right)_c = \frac{1+\gamma M_i^2[1-2f(L/D)]}{M_i\sqrt{2(\gamma+1)\left\{1+[(\gamma-1)/2]M_i^2\right\}}} - 1 \tag{21}$$

The results of calculations based on these solutions are presented in Fig. 3. They are shown for two typical dual-mode combustor inlet Mach numbers and for their entire respective allowable ranges of fractional mass addition, as well as for the range of $0 < 4f(L/D) < 0.10$. The latter range is based, in turn, on the likelihood that L/D will be of the order of 10 and $4f$ of the order of 0.01 for fully turbulent flow in a reasonably smooth duct and Reynolds numbers in excess of 10^6 that typify dual-mode combustor and research laboratory conditions.[2] If any substantial portion of the flow remains laminar, of course, the upper limit of $4f(L/D)$ will be considerably less.

Wall Boundary-Layer Separation

The static pressure increase resulting from mass addition for supersonic inlet flows could cause the wall boundary layer to separate even with wall friction present, and the assumptions and model of this analysis to break down. We will continue to use the elementary Stratford turbulent boundary-layer separation criterion of Eq. (6), largely for purposes of uniformity and because the presence of wall friction will be found to only cause a small perturbation to the original SMA flow.

Combining only Eqs. (6) and (20) leads to the result that

$$\left(\frac{M_e}{M_i}\right)_s = \sqrt{\frac{2-C_p-4f(L/D)}{2+\gamma C_p M_i^2}} \tag{22}$$

or, substituting this into Eq. (19), that

$$\left(\frac{\delta\dot{m}}{\dot{m}_i}\right)_s = \sqrt{\frac{1-(C_p/2)-2f(L/D)}{1+[(\gamma-1)/2]M_i^2}}\left\{1+\left[(\gamma-1)\left(1-2f\frac{L}{D}\right)+\frac{\gamma+1}{2}C_p\right]\frac{M_i^2}{2}\right\}-1 \tag{23}$$

These expressions produce a very similar conclusion to Eq. (9), namely, that

$$\left(\frac{V_e}{V_i}\right)_s = \frac{1-(C_p/2)-2f(L/D)}{1+(\delta\dot{m}/\dot{m}_i)_s} \tag{24}$$

The locus of separation points for the supersonic inlet Mach numbers can also be found in Fig. 3. This result continues to indicate that boundary-layer separation will occur before choking, for the expected range of values of $4f(L/D)$, even for turbulent flow.

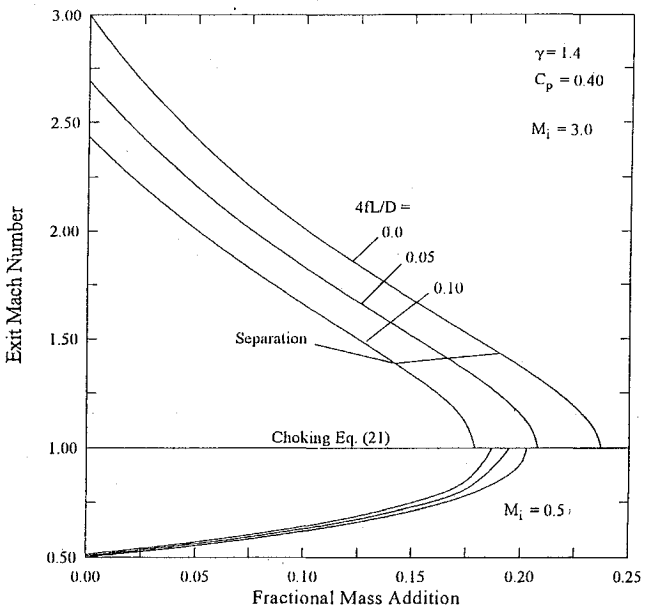

Fig. 3 Combined effects of mass addition and wall friction, $4f(L/D) = 0$ cases also appear in Fig. 1.

Most importantly, the information of Fig. 3 shows that wall friction should not have a dominant effect on the qualitative and quantitative behavior of the flow in typical experiments. The fractional mass addition for choking and separation is changed by less than 25% over the range of expected values of $4f(L/D)$.

Finally, the preceding equations Eq (24) may be combined with the definition of q to show that

$$\left(\frac{q_e}{q_i}\right)_s = 1 - \frac{C_p}{2} - 2f\frac{L}{D} \tag{25}$$

which leads to the conclusion that, regardless of the value of the inlet Mach number, q_e will always be at least about $0.8q_i$, and the average q, therefore, at least $0.9q_i$, thus supporting the earlier assertion that the local dynamic pressure does not vary much from inlet to exit.

Conclusions

This study has shown that there is a striking similarity between the influence of heat addition and mass addition on compressible flows. Most importantly, these results encourage the belief that relatively modest laboratory experiments employing mass addition can be devised that will reproduce the leading phenomena of heat addition, such as the axial variation of properties, choking, and wall boundary-layer separation. If so, the mass addition method could be further developed to explore and/or demonstrate the complex behavior of dual-mode ramjet/scramjet combustors.

Meanwhile, the insights into both types of flows found here further extend the already generous benefits of classical one-dimensional compressible flow analysis.

Acknowledgments

We are indebted to the U.S. Air Force Frank J. Seiler Research Laboratory for financial support and to the Department of Aeronautics of the U.S. Air Force Academy for its traditional hospitality and operational support of our work. The central concept for this research grew out of stimulating telephone discussions with Edward T. Curran, now Director of the Aero Propulsion and Power Directorate of the Wright Laboratory, that took place in 1992. His continuing interest in the project since then has also been of great value.

References

[1]Heiser, W. H., and Pratt, D. T., *Hypersonic Airbreathing Propulsion*, AIAA Education Series, Washington, DC, 1994, Chap. 6.

[2]Shapiro, A. H., *The Dynamics and Thermodynamics of Compressible Fluid Flow*, Ronald Press, New York, 1953, Chap. 8.

[3]Keuthe, A. M., and Chow, C. Y., *Foundations of Aerodynamics*, John Wiley, New York, 1986, pp. 413–418.

Effect of Ambient Turbulence Intensity on Sphere Wakes at Intermediate Reynolds Numbers

J.-S. Wu* and G. M. Faeth†
University of Michigan, Ann Arbor, Michigan 48109

Nomenclature

C_d	= drag coefficient
d	= sphere diameter, m
ℓ	= characteristic wake width, Eq. (2), m
Re, Re_t	= sphere and turbulence Reynolds numbers, $d\bar{U}_\infty/\nu$ and $d\bar{U}_\infty/\nu_t$
r	= radial position, m
$\bar{U}_t$	= wake-scaling velocity, Eq. (2), m/s
$\bar{U}_\infty$	= mean relative velocity of sphere, m/s
$\bar{u}$, $\bar{u}'$	= mean and rms fluctuating streamwise velocities, m/s
$\bar{v}'$	= rms fluctuating cross-stream velocity, m/s
x	= streamwise distance from center of sphere, m
ν, ν_t	= molecular and turbulence kinematic viscosities, m^2/s

Subscripts

c	= centerline value
o	= virtual origin condition
∞	= ambient condition

Introduction

RECENT studies of turbulence generation in dispersed multiphase flows have motivated the need for more information about the structure of sphere wakes at intermediate Reynolds numbers[1] ($10 < Re < 1000$), prompting earlier measurements of sphere wakes in nonturbulent environments[2] and in turbulent environments having an ambient turbulence intensity of 4.0% (Refs. 3 and 4). The observations of sphere wakes in turbulent environments indicated that whereas the wakes were turbulent, their mean streamwise velocities scaled like self-preserving laminar wakes with constant but enhanced viscosities due to the presence of the turbulence.[3] Thus, based on classical similarity analysis of self-preserving round laminar wakes with constant viscosities, the mean streamwise velocities in the wakes could be scaled as follows[3,5,6]:

$$\bar{u}/\bar{U}_t = [d/(x - x_o)]\exp(-r^2/2\ell^2) \tag{1}$$

where the wake-scaling velocity and characteristic wake width are

$$\bar{U}_t/\bar{U}_\infty = C_d\, Re_t/32, \qquad \ell/d = [2(x - x_o)/d\, Re_t]^{\frac{1}{2}} \tag{2}$$

and the effective turbulence viscosity appears in Re_t. Effective turbulence viscosities were relatively independent of position and the ratios of integral and Kolmogorov length scales to d (for the ranges 11–59 and 0.08–0.80, respectively); nevertheless, they increased with Re and exhibited low and high Re regimes separated by a transition regime where effects of vortex shedding were prominent in

Received June 27, 1994; revision received Aug. 25, 1994; accepted for publication Sept. 3, 1994.

*Postdoctoral Research Fellow, Department of Aerospace Engineering, 3000 FXB Building. Member AIAA.

†Professor, Department of Aerospace Engineering, 3000 FXB Building. Fellow AIAA.